2024 IEEE International Conference on Robotics and Automation (ICRA 2024)
May 13-17, 2024. Yokohama, Japan

Squirrel-inspired Tendon-driven Passive Gripper for Agile Landing

Stanley J. Wang[1,2], Duyi Kuang[1,3], Sebastian D. Lee[2], Robert J. Full[3], and Hannah S. Stuart[2*]

***Abstract*— Squirrels exhibit agile leaping between tree branches, often using non-prehensile gripping with compliant and passively adaptive fingers. We aim to test the utility of such gripping in agile robotic maneuvering. In the present study, we first examine the parametric design of a squirrel-inspired underactuated gripper for passive landing on impact. We fix the geometry of the gripper and vary the joint stiffness and contact conditions. We find that stiffer fingers with soft foam pads enlarge the landing sufficiency region. Specifically, friction appears to enlarge horizontal error tolerance, while joint stiffness and pad damping allow for higher impact speeds. Thus, these features should be considered in the design of future agile robot hands and feet that include high impact landings on rods with pose inaccuracy.**

I. Introduction

Mobile robotic platforms have seen a remarkable recent surge in adoption, finding their utility in unstructured environments and applications [1]. Legs provide versatility in traversing complex terrains with gaps or discrete foot holds [2]. This makes them invaluable in a wide array of scenarios ranging from search and rescue applications to exploration where terrain is particularly rough.

Many legged robots today can now reliably and repeatably complete running, jumping and landing tasks. A one-legged hopping robot called SALTO-1P can precisely control jump trajectories and achieve precise landings on a narrow foot [3]. Bipedal robot simulations such as RABBIT showcases advancements in dynamic stability with its adaptive navigation of complex terrains through the use of gait libraries and precise ground force management [4]. A quadruped robot [5] uses visual feedback to adeptly handle aperiodic and dynamic movements, making it well-suited to unpredictable terrains.

While substantial advancements have been made in legged robot navigation and control, a gap still exists between the capabilities of current walking and running legged robots and their biological counterparts. This is particularly evident when it comes to maintaining stability and agility when traversing steeply inclined, multi-oriented, and sparse substrates. Bridging this gap could allow legged robots to one day venture into entirely new terrains, potentially enabling them to maneuver through tree canopies with as much agility as squirrels.

[1] Authors contributed equally to this work
[2] Authors are with the Dept. of Mechanical Engineering, University of California Berkeley, Berkeley, CA, USA.
[3] Authors are with the Dept. of Integrative Biology, University of California Berkeley, Berkeley, CA, USA.
* Corresponding author (email: hstuart@berkeley.edu)
This paper has a supplemental video associated with it.

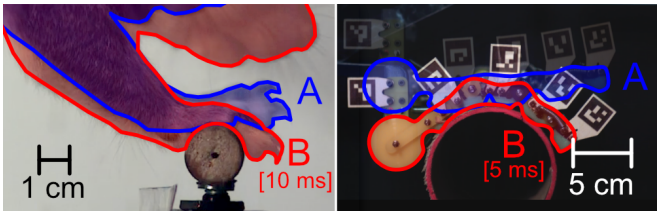

Fig. 1. Non-prehensile grasp for stable landing on a thin curved substrate exhibited by a squirrel and our robot. (a) Blue outlines denote the pose of the paw at initial contact (b) Red outlines denote the pose of the paw in a stabilized grasp, 5-10 ms after touchdown.

A. Bio-inspired Robotic Grasping and Perching

Grasping and manipulation are fundamental ways for animals to interact with their surroundings. Consequently, many roboticists have taken inspiration from these animals' dexterous behaviors to improve foot designs. For instance, SNAG [6] mimics birds' abilities to dynamically perch on complex surfaces and grasp irregular objects, emphasizing the role of passive energy transformation and underactuated grasping mechanisms. Several light-weight aerial robots tackle landing on small perching substrates by taking advantage of the Fin Ray effect observed in fish in their gripping mechanism [7]. In these relevant works, the gripper is designed to cage the branch or other object. In other works, attachment mechanisms like claws and spines are used in both prehensile [8] and non-prehensile [9] configurations for aerial landing. We now attempt to tackle high-impact landing in legged robots with an adaptable foot designed specifically for non-prehensile gripping without claws.

Different from many arboreal primates with opposable thumbs and prehensile tails, tree squirrel foot morphology includes elongated digits with ridgeless foot pads and unfused volar pads [10]. These adaptive features, coupled with the squirrels' high arboreal agility, make referencing their foot engagement during landing and walking particularly compelling. Notably, non-prehensile gripping is commonly observed when fox squirrels land on rods, as seen in Figure 1. In pilot field trials, we found initial grasp time of the squirrel to be around 10 ms [11]; this is faster than typical muscle activated reflexes [12], indicating that morphological computation plays a role in foot behavior. Therefore, we study fully-passive tendon-driven mechanical foot actuation as a means to support stable landing.

B. Overview

To address challenges in dynamic high-impact landing, we present SQRT (SQuirrel-inspired Rapid Tenodesis foot), an underactuated robotic grasper that can achieve stable landings on curved rods using a non-prehensile grasp. Section

II introduces the mechanical implementation of SQRT based on passive tenodesis actuation. In Section III, we define a static model to establish a baseline for the stability of SQRT. Section IV describes dynamic landing experiments where SQRT is dropped on a rod with varying contact locations and drop heights to understand how impact parameters affect sufficiency region. In Section V, we use motion tracking data and the static baseline to show how stable landing is affected by foot friction, damping, and joint stiffness. Section VI discusses the broader application of SQRT in agile robotic movement by emphasizing the importance of fast and robust feet. In Section VII, we conclude that this work prompts the exploration of an emerging design space towards enhanced leaping and landing capability in legged robots.

II. SQRT Foot Implementation

The SQRT grasper is designed to study mechanical features relevant to agile non-prehensile landing and grasping on curved surfaces. This testbed enables us to alter the springs at each joint and attach and detach finger pads in a modular way to explore and fine-tune individual parameters such as joint stiffness, friction, and damping.

An underactuated digit of the SQRT grasper, as shown in Fig. 2A, consists of four rigid acrylic segments connected by pin joints. The lengths of each individual segment decreases from proximal to distal (4.6, 4.0, 3.4, and 2.8 cm, respectively). We select a specific stiffness at each pin joint by attaching an extension spring, such that a resistive torque is exerted linearly with respect to joint angle. The distal joint is stiffer than the proximal and medial joints $(k_3 > k_1,\ k_2)$ so that flexion of the digit occurs at the proximal joint before distal curling. Furthermore, each joint has a hard stop or "joint lock" to prevent finger hyperextension. Finger pads are optionally included by attaching 2 cm thick high-density foam to each segment with sewing string, functioning as a proxy for the damping and elasticity properties of squirrel volar pads.[1] ArUco tags are affixed to each of the four segments to measure their motions.

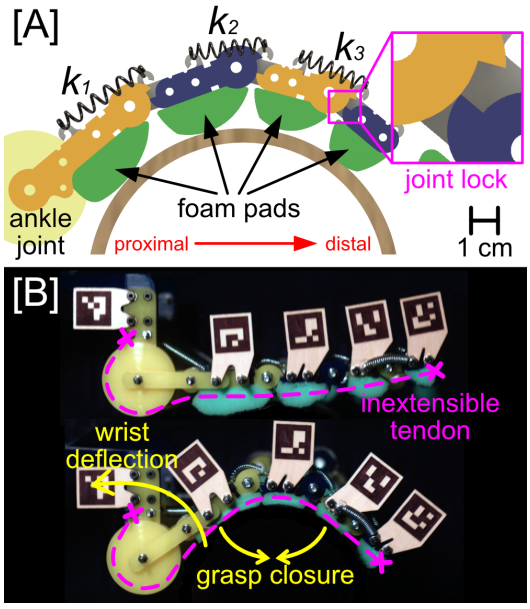

Fig. 2. Implementation of SQRT (SQuirrel-inspired Rapid Tenodesis foot). (a) Schematic of the four-segment digit with three spring-loaded joints $\{k_1,\ k_2,\ k_3\}$. Foam pads are attached for grip and damping during landing impact (b) Passive grasp actuation driven by a tenodesis action. An inextensible tendon routed through the digit allows for grasp closure to be coupled to wrist deflection.

The overall digit is driven by a tendon, as shown in Fig. 2B, which is an established mechanism for underactuated robot fingers [13]. The tendon is an inextensible string fixed at the tip of the distal digit, routed beneath each segment,[2] and subsequently affixed around a circular wheel of 2 cm radius which acts as an ankle joint. This tendon imposes a kinematic constraint (tenodesis action) on the structure where a deflection of the ankle causes a closure of the digit. This actuation mechanism allows the digit to close passively as the ankle joint rotates due to the weight of the robot and impact force of landing.

We construct a lander apparatus with SQRT digits to test its capability to passively land stably on rods whose circumference is at least double of the finger length. SQRT consists of two identical tendon-actuated digits arranged in parallel 8 cm apart to prevent out-of-plane tipping and approximate a 2D landing case. A mass is attached above the foot such that the center of gravity G is positioned approximately over the center of the digits. The overall weight of this assembly is $M = 1.5$ kg.

III. Model of Static Balancing

Understanding the stability of our lander in a static pose on top of the rod allows us to compare dynamic landing performance to the best case passive balancing scenario as a baseline. The static model of a stable grasp is shown in Fig. 3. We observe that the most proximal and most distal digits are often dominant in forming a stable grasp around the rod. We therefore simplify the grasp as two frictional point contacts (P_1, P_2). The gravitational force on our lander F_g is lumped into a point mass at G. Note that triangle

[1] We do not match any specific physical characteristics of real volar pads. We only look at the introduction or absence of compliant pads.

[2] The effective moment arm at each interphalangeal joint is 0.75 cm

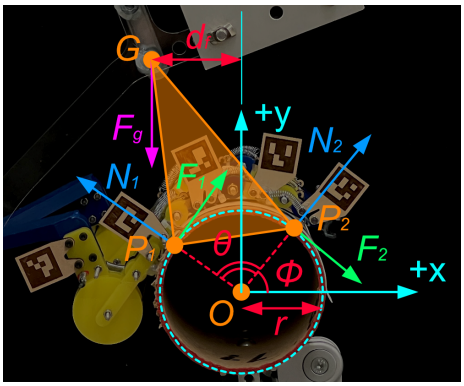

Fig. 3. 2D static model for stable grasping of SQRT on a cylinder. The grasp is simplified as two frictional point contacts (P_1, P_2) around a circle with the center of gravity at point (G).

$\triangle P_1P_2G$ is approximated as a fixed shape, since the rod radius r and digit kinematics remain constant in our system. We parameterize the static stability margin of the model as d_f, the maximum horizontal offset of the center of gravity G from the center of the rod O.[3]

The grasp model we examine is statically indeterminate. The four unknowns are the signed magnitudes of the normal and frictional forces at each point contact, written as:

$$\mathbf{x} = \begin{bmatrix} \|\vec{N}_1\| & \|\vec{N}_2\| & \|\vec{F}_1\| & \|\vec{F}_2\| \end{bmatrix}^T.$$

Force and torque balances provide the equality constraint:

$$\begin{bmatrix} \cos(\phi+\theta) & \cos\phi & \sin(\phi+\theta) & \sin\phi \\ \sin(\phi+\theta) & \sin\phi & -\cos(\phi+\theta) & -\cos\phi \\ 0 & 0 & -r & -r \end{bmatrix} \mathbf{x} = \begin{bmatrix} 0 \\ mg \\ mgd_f \end{bmatrix}$$

which uses the kinematic contact angles ϕ (angle between $\hat{x}$ and $\vec{N}_2$) and θ (angle between $\vec{N}_2$ and $\vec{N}_1$) to relate the contact forces in reference to the object's surface to those in the Newtonian frame. Note that friction force is limited by the friction coefficient μ between the grasper and substrate:

$$\|\vec{F}_i\| \leq \mu \|\vec{N}_i\|, \quad i = 1, 2$$

Furthermore, we impose a constraint on the normal force magnitude based on the system's weight:

$$\|\vec{N}_i\| \leq mg$$

This serves as a simplified approximation for limiting grasp strength due to the nature of our tenodesis mechanism. These lead us to develop further inequality constraints as:

$$\begin{bmatrix} -\mu & 0 & -1 & 0 \\ -\mu & 0 & 1 & 0 \\ 0 & -\mu & 0 & -1 \\ 0 & -\mu & 0 & 1 \\ 1 & 0 & 0 & 0 \\ 0 & 1 & 0 & 0 \end{bmatrix} \mathbf{x} \leq \begin{bmatrix} 0 \\ 0 \\ 0 \\ 0 \\ mg \\ mg \end{bmatrix}$$

For a given friction coefficient, we test for the existence of one or more solutions with varying rotational orientation ϕ to ascertain the range of d_f yielding stable static force solutions. Fig. 4 shows the range of stable d_f, assuming a constant rod diameter of 11 cm. We observe that sufficient friction plays a critical role in expanding the static stability range, but offers diminishing returns at higher values.

[3]Assuming a right handed basis, d_f is positive for rotation about $-\hat{z}$, and negative for rotation about $+\hat{z}$.

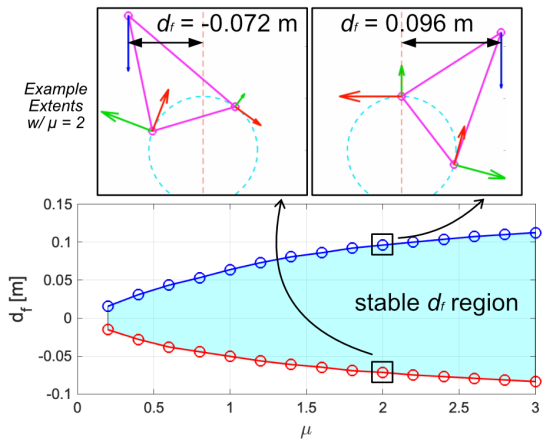

Fig. 4. Modeled static stability ranges d_f by friction coefficient μ.

IV. Experimental Methods

A. Variation of Mechanical Parameters

We examine three parameters of interest: (1) contact friction, (2) damping of pads, and (3) stiffness of digit joints. (1) is motivated by the static sufficiency region model. (2) is motivated by the hypothesis that soft volar pads, like those on squirrel feet, play a role in stable non-prehensile landing. (3) is tested because overall digit stiffness trades off the ease of passive curling with natural frequency, which influences final foot pose and bouncing of the toes during dynamic impact.We examine six testing conditions as given in Table I to explore various permutations of these design parameters.

TABLE I
SQRT Digit Test Conditions

Test	Joint Stiffness $[N/m]$			Configuration		
	k_1	k_2	k_3	Grasper	Substrate	μ
A	20	22	70	No Pad	Cardboard	0.2
B	20	22	70	No Pad	Rubber Tape	2.2
C	20	22	70	Foam Pads	Grip Tape	3.0
D	37	40	140	No Pad	Cardboard	0.2
E	37	40	140	No Pad	Rubber Tape	2.2
F	37	40	140	Foam Pads	Grip Tape	3.0

Joint stiffness is varied by swapping the springs at each joint, with tests (D, E, F) having approximately double the stiffness of tests (A, B, C). Damping is varied through inclusion (C, F) or exclusion (A, B, D, E) of foam pads on the SQRT digit. Friction is varied through the application of different materials to the surface of the landing rod, and is also influenced by the foam pads. While varying friction on the grasper directly may be more practical in field settings, it is quicker to vary the substrate properties directly in these experiment. Trials where low friction was desired (A, D) were performed with the smooth cardboard surface of the rod. For trials without pads (B, E), a soft rubbery tape is applied to the rod to ensure sufficient friction with the acrylic mechanism. For trials with foam pads (C, F), a 60 grit grip tape is applied to the rod to ensure adequate friction. The friction coefficient for each configuration is experimentally determined. The rod size is always kept constant at a diameter of 11 cm, approximating the same length scale between squirrel toes and branches found in natural arboreal habitats.[4]

B. Static Baseline Measurement

Static experiments are conducted with each unique friction configuration, based on grasper and substrate materials. This serves as validation of our static model, and establishes

[4]We leave flat, small, and irregular landing surfaces for future work.

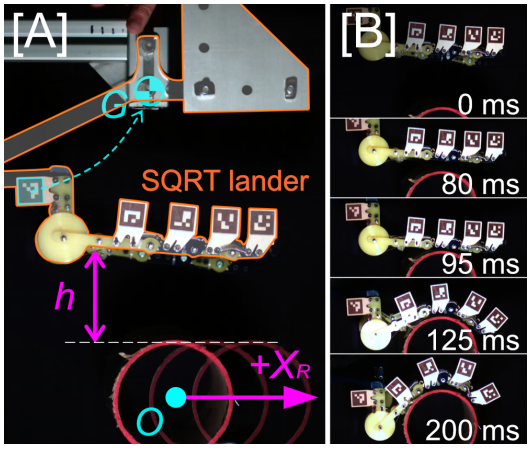

Fig. 5. (a) Experimental apparatus for vertical impact of the lander with a curved rod. Horizontal position of the rod (X_R) and drop height (h) are varied. (b) Sequence of a characteristic drop and stable landing.

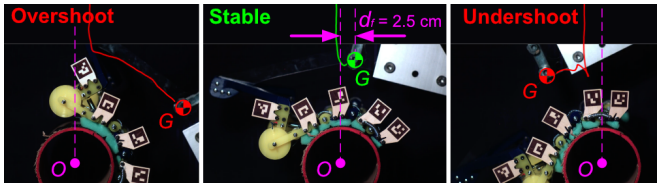

Fig. 6. Characteristic center of gravity (CG) trajectories during landing showing overshoot, stable landing, and undershoot behavior.

an additional experimental baseline of comparison with dynamic landing results. To measure the maximum extents of static stability, we place the SQRT assembly on top of the rod by hand such that the digits fully conform to the rod's surface, and slowly push it forwards or backwards until the assembly falls off. The trials are recorded by video and d_f is measured using the extracted location of point G. Multiple trials are repeated with each condition to validate this range.

C. Dynamic Landing Experiments

Dynamic landing experiments are conducted by dropping the SQRT grasper onto the rod from a given drop height (h) and rod location (X_R). These initial conditions are varied using an adjustable 80/20 aluminum frame, as shown in Fig. 5A. SQRT begins held in a 5 cm vertical linear rail by hand. Once released, it accelerates vertically downward in the rail, exits the rail and enters freefall, before impacting the rod. Drop height h is measured as the distance between the top of the landing rod and position of the SQRT digit at release. The contact location $X_R = 0$ is defined where the points G and O are vertically aligned along the $\hat{y}$ direction before SQRT is released.

A high-speed camera (Phantom V10, Vision Research) records each landing sequence at 978 frames per second. Fig. 5B shows the sequence for a characteristic stable landing consisting of release (0 ms), freefall, initial contact (95 ms), initial grasping (125 ms), and complete static stabilization (200 ms). OpenCV is used to track the poses of each ArUco tag attached to the digit. The base tag at the wrist of the digit is used to estimate the location of the center of gravity G.

Landing stability is defined by the overall trajectory of the center of gravity G, as shown in Fig. 6. A characteristic stable landing consists of the settling of G to a static pose above the rod, while unstable landings result in the deviation off the rod (overshoot/undershoot). For stable landings, we measure d_f, the offset of G from the center of the rod O once a static pose has been achieved. This offers a connection back to the stable static poses given by static experimentation and modeling (Section III). For unstable landings, d_f is recorded as the last recorded position of G, about 200-300 ms after touchdown; in these cases, the term d_f does not represent a static pose since G remains in motion until SQRT slides off.

We borrow the term "sufficiency region" as introduced in [6] to denote a range encompassing a particular parameter space where stable landings occur. We vary (h) from 10 to 40 cm and (X_R) from -2 to 3 cm. For each condition of drop height and contact location tested, we perform 5+ trials to observe stability. We utilize motion tracking to then determine the static stability range by measuring the post-landing d_f across all trials.

V. Laboratory Results

The landing sufficiency region in terms of initial conditions for each configuration is plotted in Fig. 7. We observe some initialization conditions where repeated trials exhibited both stable and unstable landings, which we denote as marginally stable, resulting in three different types of regions in these plots. In condition A – with minimal friction, no damping, and weak joint stiffness, SQRT stably landed only from a 10 cm drop height at X_R of -1.5 cm. Introducing increased friction with rubber grip tape in condition B expanded horizontal landing sufficiency region by 150%, ranging from -1 cm to 1 cm and allowing stable drops up to 20 cm in height. With the addition of damping pads in condition C, the stable touchdown range grew horizontally by 40% at 10 cm drop heights and accommodates stable drops as high as 30cm. Doubling joint stiffness in all conditions – comparing A, B, C to D, E, F, respectively – resulted in increased stability at higher drop heights. Specifically, Condition D exhibited a 200% drop height increase over A, E saw a 50% increase over B, and F saw a 30% increase over C. Only the condition with the largest stiffness, friction, and damping (F) performs stable landings at a height of 40 cm.

We translate data from the input test parameters into impact speed and final post-landing static posture in Fig. 8. Examining the maximum stable impact speed observed for each condition, we see analogous trends to drop height; this is expected as height should be directly related to impact speed after free fall. Both damping and joint stiffness play a role in increasing stability for higher impact speed landings. The range of d_f for stable dynamic landing trials appears largely independent of impact speed until a maximum tolerable speed in A, B, D, and E. At these lower speeds, there is agreement between the empirical static stability range, denoted in dashed vertical lines, and dynamic landing successes. At higher impact velocities, the recorded position after 200-300 ms may remain within the static balance range,

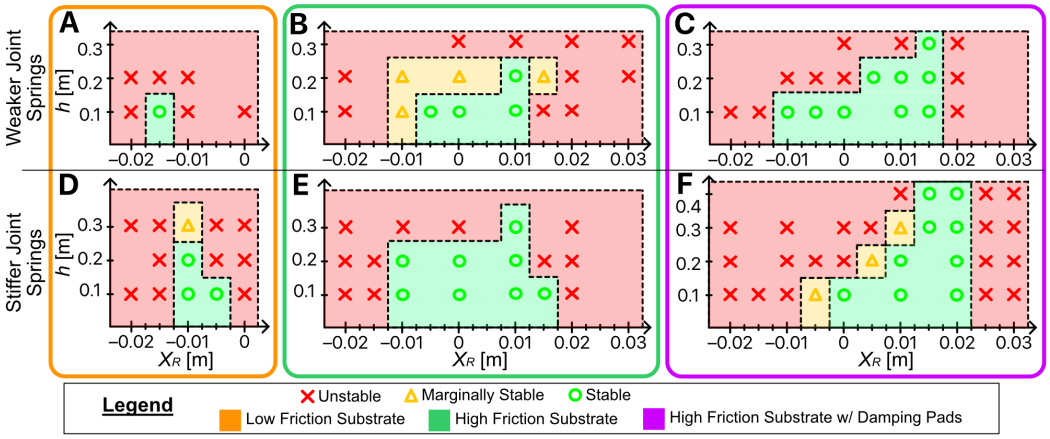

Fig. 7. Landing sufficiency regions given by observed stable, unstable, and marginally stable initial conditions at varying rod locations (X_R) and drop heights (h). Each of the columns denote a particular combination of friction/damping, while each row represents a particular joint stiffness configuration.

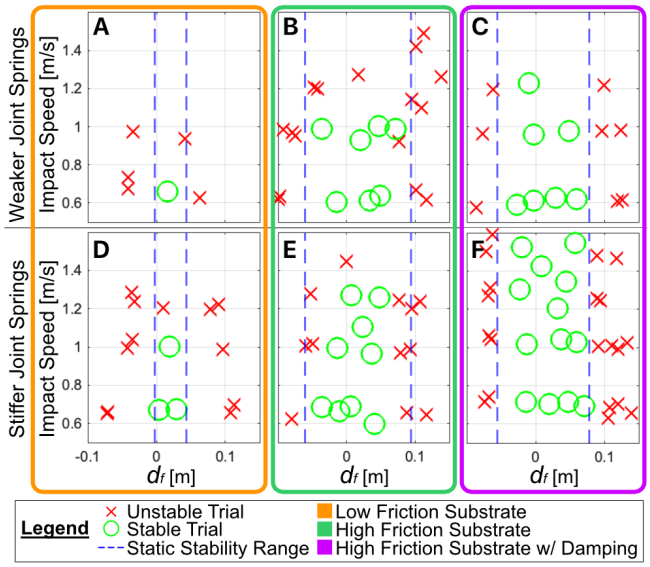

Fig. 8. Motion capture data from all dynamic landing trials showing impact velocity and final recorded pose (d_f).

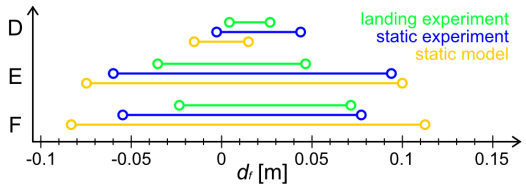

Fig. 9. Static stability bounds obtained from (1) stable dynamic landing experiments, (2) static experiments, and (3) static modeling

but SQRT still eventually slides off of the rod. This indicates that there is ongoing movement, likely in vertical bouncing, since horizontal movement is small.

The sufficiency range d_f is reported in Fig. 9 for static modeling, static experiments, and stable dynamic landing experiments. At higher friction configurations ($\mu \geq 2$ in E, F), we see the static model providing the most generous estimation of static bounds, of which the experimental data is strictly a subset. The static stability range from dynamic landing experiments is always a smaller subset of the static experiment in all cases (D, E, and F), which we attribute to the presence of dynamic effects. Discrepancies between model and experiment are most pronounced at the low friction configuration ($\mu = 0.2$ in D). This is expected as the static model will be more sensitive to small variations in friction measurement error as friction decreases.

VI. Discussion

A. Mechanical Parameters in Landing Stability

The sufficiency region trends from dynamic landing experiments lead us to postulate the role of different mechanical parameters in achieving landing stability.

We propose that friction is the dominant factor in determining the range of achievable static poses after landing. Fig. 8 shows that the range of stable postures achievable after landing is strictly bounded by the range established in static experiments. Furthermore, Fig. 9 highlights that a simple static model can be adequate in approximating these static bounds. This is useful in generalizing the determination of stable landing poses based solely on geometry and friction properties of a given grasper on a given substrate–without the need for physical experimentation.

Dynamic stabilization occurs within the initial 50-100 ms sequence immediately following landing impact. This regime is particularly challenging in robotic landing, since the rapid timescale can exceed the capabilities of active control and actuation [14]. Robustness to landing can alternatively be embodied in mechanical design parameters. In our experiments, we see that the shock absorption capability of our system – embodied by joint stiffness and addition of damping pads – influences dynamic stabilization. Examining trends in tolerable drop height/impact velocity, we see the presence of either adequate stiffness or damping help in managing energy dissipation and preventing destabilization after impact. We associate this with decreased rebound and release of the grasp due to bouncing, leading to increased engagement with the substrate and the convergence towards a stable static pose.

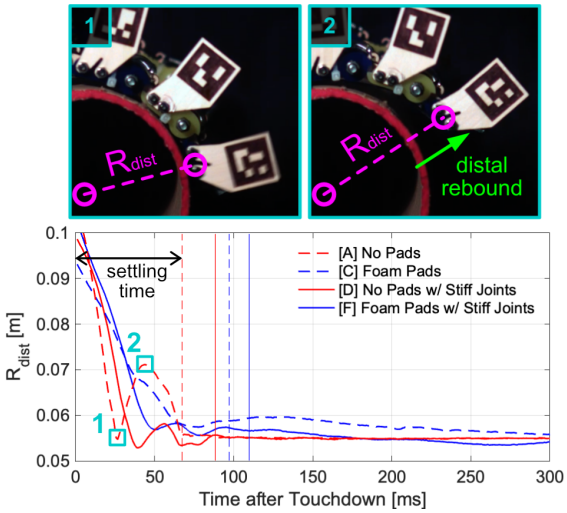

Fig. 10. Rebound of the distal phalanx characterized by its radial distance (R_{dist}). Characteristic trials at 10 cm drop height are shown for tests A, C, D, F to illustrate the effect of joint stiffness and damping pads.

B. Distal Phalanx Rebound

An initial attempt at quantifying dynamic stabilization is conducted by examining the rebound movement of the distal phalanx after touchdown. We quantify the magnitude of rebound by examining the maximum variation in the radial distance of the distal phalanx relative to the rod R_{dist} in the first 150 ms following touchdown, after the first local minimum. Fig. 10 shows plots of distal distance for four example trials conducted at the 10 cm drop height. We see that the introduction of either stiffened joints (test D) or damping pads (test C) reduced distal rebound compared to the baseline (test A).

To isolate the effect of joint stiffness, we conduct comparative statistical analysis across all trials at drop heights under 30 cm between Tests A and D. The average rebound magnitude observed in D is significantly lower than A ($p = 0.004$). Thus, we see manipulation of joint stiffness alone led to notable reductions in distal rebound, in addition to an expansion of stable landing heights. There is also a statistically significant difference between the distal rebound magnitude for Tests A and C ($p = 0.008$) and Tests A and B ($p = 0.003$), indicating that either or both friction and damping also play a role in reducing rebound.[5]

C. Ungrasping Demonstration

We expect that one advantage of using non-prehensile grasping in agile robots is to both grasp and ungrasp quickly without substantial digit reorientation or control. The SQRT digit is capable of quickly flexing and conforming around a curved substrate, but can also easily disengage rapidly when a grasp is no longer desired. We conduct a demonstration showing a body-weight-driven engagement and disengagement, emulating a landing and taking-off sequence. The SQRT lander is dropped vertically onto the rod while attached to an elastic bungee from above. As shown by Fig. 11, grasp engagement occurs within the first 100 ms after touchdown. Subsequent disengagement occurs on a similar time scale, with complete release of the rod in 60 ms.

[5]We cannot isolate damping from friction given our test conditions, so we cannot assert that either factor alone decreases distal rebound.

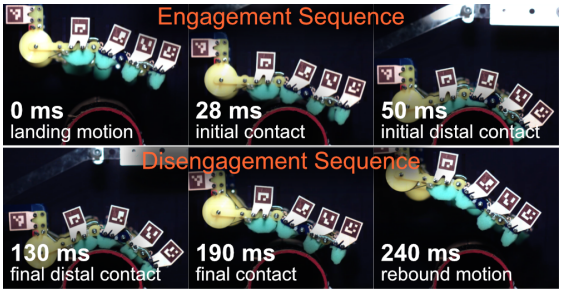

Fig. 11. Demonstration of SQRT's rapid grasp-to-ungrasp capability.

We believe this work motivates the use of passive non-prehensile grasping to swiftly disengage from substrates, facilitating seamless transitions to subsequent movements without the need for foothold or pose adjustments. By incorporating minimal active control components, this adaptability can be optimized to sequence multiple actions consecutively–like bounding through the treetops–in future work.

VII. Conclusion

Our squirrel-inspired passive lander, SQRT, quickly adapts to a rod, applying a non-prehensile grasp to support stable, passive landing. We focus here on non-prehensile gripping to emulate a common grasp type that enables squirrels to achieve agility, especially when navigating irregular surfaces and enduring high-impact locomotion. While there is a clear distinction between a squirrel's complex multi-limb landing and our robotic grasper's vertical landing and simplified implementation, our experiments provide a foundation for refining foot design aimed at sparse terrain navigation. In particular, we found that joint stiffness, friction, and inclusion of damping finger pads can all play a role in landing stability on rods. This emphasizes the diverse end-effector design possibilities in the realm of agile legged robots.

A. Future work

There are promising future pathways to expand the capabilities of SQRT. One next step is to further decode the role of dynamic rebound, further optimizing the design parameters introduced in this work to reduce this effect at high velocity cases. Another step lies in expanding the stability envelope beyond our baseline tests by adding active mass adjustment. For example, the addition of an accelerometer and torque-generating reaction wheel could allow for the development of an active stabilization technique. Combined with the passive capabilities demonstrated, this would further augment landing robustness and stability. Ultimately, we envision the application of SQRT towards enhancing the agility of existing legged robots. This will involve investigating further the design of volar pads and the role of non-prehensile grip for both grasping and ungrasping speed and stability.

Acknowledgment

Work funded by a Multidisciplinary University Research Initiatives (MURI) grant, ARO #W911-NF-1810327.

REFERENCES

[1] P. Biswal and P. K. Mohanty, "Development of quadruped walking robots: A review," *Ain Shams Engineering Journal*, vol. 12, no. 2, pp. 2017–2031, 2021.

[2] Q. Nguyen, A. Agrawal, W. Martin, H. Geyer, and K. Sreenath, "Dynamic bipedal locomotion over stochastic discrete terrain," *The International Journal of Robotics Research*, vol. 37, no. 13-14, pp. 1537–1553, 2018.

[3] J. K. Yim, B. R. P. Singh, E. K. Wang, R. Featherstone, and R. S. Fearing, "Precision robotic leaping and landing using stance-phase balance," *IEEE Robotics and Automation Letters*, vol. 5, no. 2, pp. 3422–3429, 2020.

[4] A. Agrawal and K. Sreenath, "Bipedal robotic running on stochastic discrete terrain," in *2019 18th European Control Conference (ECC)*. IEEE, 2019, pp. 3564–3570.

[5] A. Agrawal, S. Chen, A. Rai, and K. Sreenath, "Vision-aided dynamic quadrupedal locomotion on discrete terrain using motion libraries," in *2022 International Conference on Robotics and Automation (ICRA)*, 2022, pp. 4708–4714.

[6] W. R. Roderick, M. R. Cutkosky, and D. Lentink, "Bird-inspired dynamic grasping and perching in arboreal environments," *Science Robotics*, vol. 6, no. 61, p. eabj7562, 2021.

[7] K. Broers and S. Armanini, "Design and testing of a bioinspired lightweight perching mechanism for flapping-wing mavs using soft grippers," *IEEE ROBOTICS AND AUTOMATION LETTERS*, vol. 7, pp. 7526–7533, 2022.

[8] H. Jiang, M. T. Pope, E. W. Hawkes, D. L. Christensen, M. A. Estrada, A. Parlier, R. Tran, and M. R. Cutkosky, "Modeling the dynamics of perching with opposed-grip mechanisms," in *2014 IEEE international conference on robotics and automation (ICRA)*. IEEE, 2014, pp. 3102–3108.

[9] A. Lussier Desbiens, A. T. Asbeck, and M. R. Cutkosky, "Landing, perching and taking off from vertical surfaces," *The International Journal of Robotics Research*, vol. 30, no. 3, pp. 355–370, 2011.

[10] M. CARTMILL, "2 - pads and claws in arboreal locomotion," in *Primate Locomotion*, F. A. JENKINS, Ed. Academic Press, 1974, pp. 45–83.

[11] D. Kuang, S. Wang, S. Lee, L. Wang, and R. Full, "Kinematic paw adjustments of fox squirrels landing on curved surfaces," in *Society of Integrative and Comparative Biology Annual Meeting Exhibition Final Program and Abstracts*, 2023.

[12] D. Kosarov, "The reaction time of single motor units in the human muscle," *Agressologie*, vol. 20, no. 5, pp. 279–285, 1979.

[13] L. Birglen, T. Laliberté, and C. M. Gosselin, *Underactuated robotic hands*. Springer, 2007, vol. 40.

[14] U. Martinez-Hernandez, N. F. Lepora, and T. J. Prescott, "Active control for object perception and exploration with a robotic hand," in *Biomimetic and Biohybrid Systems*, S. P. Wilson, P. F. Verschure, A. Mura, and T. J. Prescott, Eds. Springer International Publishing, 2015, pp. 415–428.